Running head: Differential dissolution in coccolithophores

Species-specific differential dissolution morphology of selected coccolithophore species: an experimental study

Gerald Langer[1,2], Ian Probert[3], Jeremy R. Young[4], Patrizia Ziveri[1,5,6]

Affiliations

[1] Institute of Environmental Science and Technology, Universitat Autònoma de Barcelona (ICTA-UAB), Barcelona, 08193, Spain

[2] National Institute of Oceanography and Applied Geophysics - OGS, Trieste, 34151, Italy

[3] Sorbonne Université/CNRS, Roscoff Culture Collection, FR2424 Station Biologique de Roscoff, 29682 Roscoff, France

[4] Earth Sciences, University College London, London WC1E 6BT, UK

[5] Catalan Institution for Research and Advanced Studies (ICREA), Barcelona, Spain

[6] BABVE Dept., Universitat Autònoma de Barcelona (ICTA-UAB), Barcelona, 08193, Spain

Corresponding author: Gerald Langer (gerald.langer@cantab.net, gerald.langer@uab.cat)

500-character summary

Coccolithophores are important marine $CaCO_3$ producers and their biominerals, the coccoliths, partly dissolve in the upper water column where dissolution is unexpected. Studying coccolith dissolution in field samples is hampered by a paucity of experimental studies describing dissolution morphologies. Here we fill this gap by experimentally dissolving different coccolithophores and applying our results to field samples.

Highlights

- Experimental studies on biogenic $CaCO_3$ dissolution provide novel insights into field sample observations and biomineralization processes
- Experimental data aid the interpretation of aberrant coccolith morphology in field samples
- In *C. braarudii* partial dissolution reveals a nanostructure in the distal shield
- The nanostructure in *C. braarudii* requires adjustments in biomineralization models

Abstract

Coccolith dissolution in the water column is an important process in the marine carbon cycle. Identifying dissolution in water column samples has been difficult due to a lack of experimental reference datasets showing dissolution morphologies. We conducted a laboratory $CaCO_3$ dissolution experiment to detect differential dissolution morphologies of three selected coccolithophore (abundant marine calcareous phytoplankton) species, *Coccolithus braarudii*, *Helicosphaera carteri*, and *Scyphosphaera apsteinii*. These species were selected because they are ecologically and biogeochemically important (significant contributors to $CaCO_3$ production) and have been less studied than *Gephyrocapsa*. Muroliths of *S. apsteinii* dissolve faster than lopadoliths, which in turn dissolve as fast as *H. carteri* but faster than *C. braarudii*. In S. apsteinii lopadoliths, dissolution rate depends on the crystallographic orientation of the crystals. Comparison with field samples shows that experimental data are helpful when interpreting field samples. For example, we identify dissolution in water and sediment samples reported in the literature. In *C. braarudii* dissolution reveals a nanostructure on the proximal side of the distal shield, an observation that has implications for coccolith biomineralization models, which do not currently account for the formation of such a structure. This nanostructure features “units” of ca 50-100 nm and resembles the nanostructure well known from extracellular calcifiers such as molluscs and foraminifera. Whether this resemblance is underpinned by a similar formation mechanisms remains unknown, but we think this unlikely.

1) Introduction

Present anthropogenic CO_2 concentration changes, both atmospheric and marine, cannot be fully understood without considering marine calcium carbonate, largely produced by calcifying organisms (Broecker and Peng 1982, Morse and Mackenzie 1990). These calcifying organisms influence air-sea CO2 exchange in several ways, e.g. through particulate inorganic- and organic carbon production in the surface ocean but also through export of calcium carbonate to the deep ocean (Morse and Mackenzie 1990). The most productive marine calcium carbonate ($CaCO_3$) producers are pelagic organisms, with coccolithophores contributing ca. 90% of global pelagic $CaCO_3$ production (Ziveri et al., 2023) and ca. 50% of $CaCO_3$ sedimentation (Milliman 1993, Broecker and Clark 2009). Dissolution of $CaCO_3$ in the photic zone is an important process in the marine $CaCO_3$ cycle (Ziveri et al. 2023; Subhas et al. 2022; Sulpis et al. 2021). The importance of dissolution for the marine C-cycle has two main aspects. Firstly, dissolution of CaCO3 releases two moles of alkalinity per one mole of dissolved inorganic carbon, thereby shifting the seawater C-system towards higher pH values (Zeebe and Wolf-Gladrow, 2001). Secondly, the loss of ballast minerals reduces carbon export efficiency thereby influencing the C-cycle long-term (Klaas and Archer 2002). In addition to occurring in the open ocean photic zone, dissolution of carbonates in general, and coccoliths in particular, may also occur in sediments and coastal CO_2 vent sites (Honjo 1975, Ziveri et al 2014).

Assessing coccolith dissolution in these diverse settings can be challenging, but partial dissolution morphologies as identified in electron micrographs have proved a useful tool (e.g. Langer et al 2007, Ziveri et al 2014). Knowledge of such differential dissolution morphologies will aid interpretation of field samples, e.g. the degree of dissolution in one species will inform inferences about the degree of dissolution in other species. More fundamentally, knowledge about dissolution morphologies will enable us to accurately distinguish malformation / under-calcification from dissolution, which is not necessarily an easy task (Young 1994). Finally, dissolution might reveal informative structural features (Langer et al 2007). The main goal of our study is to provide a dissolution-morphology reference dataset which can be used to identify dissolution in water column samples. The applicability of our data to sediment samples might be more limited as discussed below. The interpretation of field samples is difficult, however, because the degree, and even the mere fact, of dissolution often need to be inferred from

the micrographs alone, without precise knowledge of the physico-chemical conditions leading to the observed morphology. For example, in surface sediments *Calcidiscus leptoporus* coccoliths (placoliths characterized by two shield-like plates connected by a central tube) lacking proximal shields have been taken as a sign of heavy dissolution (Roth and Berger 1975), which has been proposed as a proxy for dissolution in the sedimentary record (Matsuoka 1999). Only an experimental study could show that separation of the shields is the first observable dissolution feature occurring at less than 8% mass loss (Langer et al 2007) revealing the "weak spot" at the proximal end of the tube (the position of the proto-coccolith ring, Young et al 2004).

Despite the importance of experimental studies showing graded dissolution of coccoliths, only a few such studies have been conducted (McIntyre & McIntyre 1971, Burns 1977, Kleijne 1990, Henriksen et al 2004, Langer et al 2006b, Holcová and Scheiner 2023), with a focus on *Gephyrocapsa spp*, in particular *G. huxleyi*, a widely used model species (Wheeler et al 2023).The degree of dissolution in G. huxleyi water column samples is difficult to assess as there are variations of progressive dissolution patterns with e.g. warm- and cold-water phenotypes (Burns 1977). The latter author pointed out that a tropical G. huxleyi loses the central grille in the first stages of dissolution, while a cold-water phenotype does not. Calcite removal from the long margin of the radial elements is a sign of early dissolution in the cold-water phenotype but not in a heavily calcified phenotype. These and similar observations made by Burns (1977) show that assessing the degree of dissolution in G. huxleyi is not an easy task and morphotype-specific assessments are required. While *G. huxleyi* is numerically the most abundant coccolithophore in present oceans, its contribution to coccolithophore $CaCO_3$ production is rivalled by some genera with larger coccoliths, such as *Calcidiscus* and *Coccolithus* (Wheeler et al 2023). The relatively recent appearance of *G. huxleyi* in the fossil record implies that this species is not applicable to deep time sediment core studies (Henderiks et al 2022). It is therefore worthwhile also studying genera with larger coccoliths and mass, biogeochemically important (Ziveri et al., 2004), and with a more extensive evolutionary history, e.g. *Coccolithus*, *Helicosphaera*, and *Scyphosphaera* (Henderiks et al 2022). The latter genera are not as abundant as *E. huxleyi* but play an important role in coccolithophore CaCO3 production and export in modern oceans (Baumann et al., 2004; Daniels et al., 2014, 2016; Gafar et al., 2019; Ziveri et al., 2007).

Based largely on field sediment studies, it is accepted that some coccolith forms dissolve faster than others. While *G. huxleyi* and *Umbilicosphaera sibogae* are among the fast-dissolving placolith bearing species, *G. oceanica*, *C. leptoporus*, and *C. pelagicus* are comparatively slow-dissolving (McIntyre & McIntyre 1971, Berger 1973, Roth and Coulbourn 1982). These studies have not assessed how dissolution morphologies of different species relate to each other. In other words, which dissolution morphology of species x corresponds to a given dissolution morphology of species y?

Coccoliths contain crystals of different orientations, sizes, and shapes. A typical feature, for example, is the presence of crystals with radial c-axis orientations (R-units) and others with vertical c-axis orientations (V-units, Young et al 1992). It might therefore be hypothesized that different crystals display different structural features, not only on the micrometre but also on the nanometre scale. Some of these features might only be discernible in partially dissolved specimens.

In this study we selected laboratory cultures of *Coccolithus braarudii*, *Helicosphaera carteri*, and *Scyphosphaera apsteinii*, and performed a dissolution experiment to follow their differential dissolution morphologies by means of sequential sampling for SEM analysis. Here we analyse two important aspects of dissolution. Firstly, the selective dissolution of different species relative to each other. Secondly, the evolution of morphology of a given species with progressive dissolution. We hypothesize that dissolution morphologies will be different from malformations (Bianco et al 2025, Langer et al. 2006, Langer et al 2021, Gerecht et al 2015, Meyer et al 2020) and therefore a dissolution reference dataset will enable us to unambiguously identify dissolution in field samples. The experimental setup chosen here is ideally suited to analyse sequential dissolution morphology with nanometric resolution. This enables the identification of different dissolution stages in field samples, providing additional information over and above the mere distinction of dissolution features and malformations.

Experimental dissolution studies provide a good source of information on the evolution of morphology with dissolution, without confounding factors from field studies such as variance in the primary biomineralization morphology.

2) Material and Methods

157 2.1) *Culture conditions*

158 Clonal cultures of *Coccolithus braarudii* (strain RCC1198), *Scyphosphaera*
159 *apsteinii* (strain RCC3598), and *Helicosphaera carteri* (strain RCC1323) were grown in
160 aged (3 months), sterile-filtered (Stericup-GP Sterile Vacuum Filtration System, 0.22 µm
161 pore size, polyethersulfone membrane, Merck) natural surface seawater sampled in the
162 English Channel off Roscoff, France, enriched with 288 µM nitrate, 18 µM phosphate,
163 and silicate, trace metals, and vitamins as in K/2-I (https://roscoff-culture-
164 collection.org/medium-id/k2-i). All strains were obtained from the Roscoff Culture
165 Collection (http://www.roscoff-culture-collection.org).

166 Cultures were grown under a 16:8 h light:dark cycle at a light intensity of
167 50 µmol photons m^{-2} s^{-1} in temperature-controlled culture incubators. *Coccolithus*
168 *braarudii* RCC1198 was grown at 15°C, while *Scyphosphaera apsteinii* RCC3598 and
169 *Helicosphaera carteri* RCC1323 were grown at 20°C. Cells were grown in dilute batch
170 cultures, ensuring a quasi-constant seawater carbonate system over the course of
171 exponential growth (Hoffmann et al. 2015). Cell densities were determined by flow
172 cytometry immediately after sampling. Cultures used in the dissolution experiment were
173 initially checked by light and scanning electron microscopy to ensure that coccosphere
174 morphology was normal (as observed in light microscopy) and the percentage of
175 coccolith malformations was below 15% (as determined by SEM analysis, Langer and
176 Bode 2011). The latter is a very low percentage of malformations in cultures (in which
177 values up to 90% have been reported, Langer et al 2006, Langer et al 2013), enabling
178 this study to focus on normal coccoliths and their dissolution morphologies, as opposed
179 to the dissolution features of malformed coccoliths (Langer and Bode 2011, Langer et al
180 2013, Langer et al 2023). We chose not to analyse the dissolution morphology of
181 malformed coccoliths because results are intended to be applicable to field samples, in
182 which the percentage of malformed coccoliths is typically only ca. 2% (Langer et al
183 2006, Langer et al 2013). Analysis of the dissolution morphologies of malformed
184 coccoliths would require a different experimental setup, with cultures displaying high
185 proportions of malformed coccoliths. Such an approach would be interesting in itself,
186 but does not fall within the scope of the present study (Langer et al 2006).

187 2.2) *Dissolution experiment*

To study differential dissolution morphologies accurately, the selected species were combined in a single 2.7L bottle (Holcová and Scheiner 2023), in which case only one calcite saturation state (omega) value can be selected. In pre-experiments we found that *Gephyrocapsa huxleyi* coccoliths dissolved more than 10x faster than coccoliths of *Coccolithus braarudii*, *Helicosphaera carteri*, and *Scyphosphaera apsteinii*, meaning it was not possible to include *G. huxleyi* in our experiment. The three other species, *C. braarudii*, *H. carteri*, and *S. apsteinii*, displayed broadly similar dissolution kinetics and were therefore suited for our purpose.

To start the dissolution experiment, living cells were transferred into a 2.7L bottle containing culture medium that was acidified using calculated amounts of HCl (3.29M) immediately prior to cell transfer. We used acidification to manipulate omega calcite because it is more representative of dissolution scenarios in the field than changes in Ca concentration. Omega calcite is the saturation state of seawater with respect to calcite, with omega < 1 indicating dissolution and omega > 1 potential crystal growth. This decision is important because the manipulation of omega calcite via acidification is more effective than via Ca concentration decrease (Hassenkam et al 2011). We chose to work with living cells, as opposed to isolated coccoliths for the following reasons. Firstly, we wanted our results to be useful for comparison with various dissolution scenarios such as whole cells in copepod and micro-grazer guts, whole cells in marine snow aggregates, whole cells in ocean acidification-affected corrosive waters. Secondly, we wanted to analyse effects of dissolution on coccospheres, as opposed to only on individual coccoliths. Thirdly, removing coccoliths from cells is not always an easy task and often requires chemical or heat treatment which might alter structural integrity and organic content (Manuela Bordiga, personal communication, 2025). Since this is a pilot study, we wanted to keep the experimental setup as straightforward as possible. Follow up studies should deal with modified setups to explore additional factors influencing dissolution patterns. The culture medium prepared using natural surface seawater sampled off Roscoff, France has a typical dissolved inorganic carbon, DIC, of ca 2000 $\mu mol\ kg^{-1}$ (Johnson et al 2022). We used this value for DIC and measured pH (NBS) = 6.44 to calculate omega calcite = 0.033 using the program CO2SYS (Pierrot et al 2011). The calculated value for omega calcite (0.033) was therefore approximate. However, DIC variability of natural surface seawater sampled off Roscoff, France is low, therefore introducing only a negligible inaccuracy in calculated omega calcite in the context of

the present study, i.e. an error of ±0.005 is expected (Johnson et al 2022). The present study was not designed to analyse dissolution kinetics precisely (such as in Subhas et al 2018), meaning an approximate determination of the carbonate system is sufficient. We used a Cyberscan 500 pH meter (Eutech Instruments, UK) equipped with a Mettler Toledo InLab 413/ID67 electrode to determine pH on the NBS scale.

Experimental dissolution over a very short space of time (on the order of seconds as in Yang et al 2021) only allows for comparatively low-resolution light micrographs that would have been insufficient for our purpose. The advantage of a short experiment duration, however, is that DIC uptake and gas exchange with the atmosphere, and therefore carbonate system variability, is negligible. Our dissolution experiment, conducted over a duration of 11 hours, was carried out in the dark at 4°C to ensure that cellular metabolism (including photosynthesis and coccolith production) was severely restricted over the course of the experiment. Cell densities were 711 cells/mL for *C. braarudii*, 665 cells/mL for *H. carteri*, and 586 cells/mL for *S. apsteinii*. The resultant low overall cell density of 1963 cells/mL contributed to ensuring a quasi-constant carbonate system over the course of the experiment (Langer et al 2006, Langer and Bode 2011, Hoffmann et al 2015). Physico-chemical conditions over the course of the experiment were additionally homogenized by regular mixing, i.e. keeping the cells in suspension. No aggregation of cells occurred and no sedimentation of cells or coccoliths took place. The pH did rise by ca 0.1 over the course of the experiment, but this corresponds to an increase in omega calcite of only ca. 0.005, i.e. the same magnitude as the minor uncertainty introduced by our choice of DIC value (see above).

After the dissolution experiment was completed, cells were transferred into normal culture conditions as specified above. All three species, *C. braarudii*, *H. carteri*, and *S. apsteinii*, resumed cell division and coccolith production as confirmed by optical inspection using light microscopy. We did not quantify coccolith morphology in re-calcifying cells, but noted that initially coccoliths seemed to display more malformations than prior to the dissolution experiment. This assessment is based on an informal analysis by means of light microscopy; no images were taken.

Multiple (15) sequential samples for detailed morphological analysis were taken over the 11 hour duration of the experiment. Samples for SEM analysis were filtered onto polycarbonate filters (0.8 µm pore-size), dried in a drying cabinet at 50°C for 24 h, then sputter-coated with gold–palladium using a Cressington 108 sputter coater (Cressington

Scientific Instruments, Watford, UK). Imaging was performed with a Phenom Pro desktop SEM at the Station Biologique de Roscoff, France, and an El SEM Zeiss Merlin at UAB, Barcelona, Spain. All the morphological features described in this study are discernible using the Phenom Pro desktop SEM. We used the Zeiss Merlin FE-SEM only to produce images showing the nanostructure on the proximal side of the distal shield of C. braarudii because the latter microscope has a higher resolution. This nanostructure, however, was discovered using the Phenom Pro desktop SEM. An average of ~350 coccoliths was analysed per sample (Langer and Benner 2009). To describe dissolution morphologies, we selected conspicuous features that could be easily followed over the course of the experiment to ensure robust results and to facilitate application to field samples. In *C. braarudii* and *H. carteri* we analysed dissolution features of coccospheres in addition to dissolution features of coccoliths. In *S. apsteinii* only dissolution features of coccoliths were analysed because coccospheres in this species lack the mechanical stability needed to consistently withstand the mechanical forces experienced in SEM preparation (Langer et al 2023). The following morphological features were used to describe dissolution. In *C. braarudii*: 1) etching of the inner tube, 2) etching of the distal shield, 3) central area bar missing, 4) coccoliths broken, 5) gaps in coccospheres, 6) coccospheres collapsed, 7) nanostructure visible (on proximal side of distal shield). In *H. carteri*: 1) etching, 2) coccoliths broken, 3) coccospheres collapsed. In *S. apsteinii* lopadoliths: 1) etching of base, 2) etching of barrel, 3) rim serrated, 4) lopadoliths broken, 5) isolated lopadolith V units. In *S. apsteinii* muroliths: 1) centre missing, 2) etching, 3) muroliths broken. Scanning electron micrographs of all of these features are shown in Figs 1-5.

3) Results and Discussion

3.1) Differential dissolution: general observations

We subjected living cells of three common coccolithophore species, namely *Coccolithus braarudii*, *Helicosphaera carteri*, and *Scyphosphaera apsteinii*, to seawater undersaturated with respect to calcite, i.e. omega calcite ca. 0.033 (see Methods). The duration of the experiment was 11 hours, at the end of which only a few isolated distal shield elements of *C. braarudii* remained (Fig 6). Our observation that *C. braarudii* is more dissolution resistant than *H. carteri* tallies well with conclusions drawn from

studying Atlantic Ocean floor sediments (Berger 1973). Information on *S. apsteinii* in differential dissolution studies is rare, with this species either only mentioned but not discussed or not mentioned at all (McIntyre & McIntyre 1971, Berger 1973, Roth and Coulbourn 1982). From our data we conclude that *S. apsteinii* lopadoliths display dissolution kinetics similar to *H. carteri*, while *S. apsteinii* muroliths dissolve faster. *S. apsteinii* lopadolith R-units lopadolith R-units, the smaller radial crystals, conspicuously dissolve faster than V-units, the larger vertical crystals (Figs 6, 7), potentially as a result of the size difference of the individual crystals, with V-units being larger (see also Drescher et al 2012). The different dissolution kinetics of V and R units in the same lopadolith illustrates that the microstructure of a $CaCO_3$ biomineral influences dissolution kinetics, which could not be inferred from its polymorph alone (the only polymorph that lopadoliths contain is calcite; Walker et al 2024, Langer and Ziveri, in press). Both etching and broken coccoliths appear simultaneously in *S. apsteinii* lopadoliths and *H. carteri* (Figs 6, 7). In *C. braarudii* etching of the inner tube occurs simultaneously with etching in *H. carteri* and *S. apsteinii*, but etching of the *C. braarudii* distal shield appears later, possibly because the latter features the largest crystals (Figs 6, 7). Relatively slow dissolution of the distal shield compared to the tube/central area was also observed in *C. leptoporus* and might be a general feature of Coccolithales placoliths (Langer et al 2007).

3.2) Comparison with field samples

Identification of dissolution in field samples:

As noted in the introduction coccolith dissolution in the water column is being highlighted as a key process, greatly affecting the export production of coccolith $CaCO_3$ to the bottom sediment. Our experimental results on the sequence of dissolution stages might usefully be applied to study of field samples in order to analyse and track water column dissolution. As a proof of concept we show here (Fig 8) images of *Coccolithus braarudii* and *Helicosphaera carteri* coccoliths from sediment trap samples and of coccoliths from water column samples, in both cases showing dissolution features directly comparable to those we observed experimentally. It is also noteworthy that the nanostructure seen in the experimental samples is visible in the field samples (Fig 8) showing that it is not an experimental artefact. Comparable dissolution features have also been illustrated in the literature, for example by Cubillos et al (2012) and Kleijne (1990), although in some cases they have been ascribed to malformation.

It is striking that in the three species studied here dissolution morphologies are clearly different from malformations. The latter do not resemble etching as described here (Figs 1-5). This is remarkable considering that it has typically been difficult to distinguish dissolution from malformation, and even fracture, in G. huxleyi (McIntyre & McIntyre 1971, Burns 1977, Kleijne 1990, Holcová and Scheiner 2023, Young 1994, Langer et al 2006b, Langer and Benner 2009, Langer et al 2011). These difficulties in identifying dissolution morphology in G. huxleyi are particularly conspicuous in morpho-type B/C, but are clearly noticeable in type A as well (own observations, unpublished). It might be speculated that dissolution is easier to identify in type R because the latter features fused distal shield elements which makes the overall morphology more similar to the one of the species studied here. This conjecture is supported by G. huxleyi morphotype-specific dissolution morphologies described in water column samples (Burns 1977). It will be worthwhile studying different G. huxleyi morphotypes in greater detail. Species-specific dissolution features such as the serrated rim in S. apsteinii lopadoliths are also dissimilar to malformations such as type R (Langer et al 2021, Langer et al 2023). The nanostructure on the proximal side of the distal shield of C. braarudii is hardly visible in normal as well as malformed coccoliths, whereas it is clearly visible in partially dissolved coccoliths. In C. braarudii a concentric hole sometimes appears in malformed coccoliths (Langer et al 2021). This hole is clearly different from etch pits. A typical feature of more severe malformations in placolith bearing species is the distorted architecture of the shields (Bianco et al 2025, Langer et al 2006, Langer and Benner 2009, Langer et al 2011, Langer and Bode 2011, Langer et al 2012, Langer et al 2013, Langer et al 2021, Langer et al 2023, Kottmeier et al 2022, Gerecht et al 2015, Milner et al 2016, Johnson et al 2022) which does not occur as a result of dissolution.

Do the conditions under which dissolution occurs influence dissolution morphologies?

As a caveat we will say that dissolution morphologies might well depend on the conditions under which dissolution occurs. For example, the presence or absence of an organic coating around coccoliths results in slightly different dissolution morphologies as seen in high resolution AFM imaging (Henriksen et al 2004). Since we did not remove the organic coating, our results should be best applicable to water samples (with organic coating) as opposed to sediment samples (in which the organic coating might be degraded). That said, the organic coating of coccoliths can still slow down dissolution

after 70Ma in the sediment (Sand et al 2014). Whether dissolution morphologies of these ancient coccoliths would be similar to those of cultured specimens remains to be tested. A good candidate would be *C. pelagicus* because it first appeared in the fossil record more than 60 Ma (Henderiks et al 2022). Another aspect to consider is the way undersaturation is achieved. Dissolution kinetics in low-Ca solutions are different from those in low-pH solutions (Hassenkam et al 2011). It is an open question whether dissolution morphologies would differ too. In addition, pressure-driven undersaturation might be relevant for deep-sea sediment samples. All of these issues are amenable to experimental testing and should be the focus of future studies.

3.3) Structural integrity of the coccosphere

An interesting difference between *C. leptoporus* (Langer et al 2007) on the one hand and *C. braarudii / H. carteri* (this study) on the other hand is the structural integrity of coccospheres under dissolution. The earliest feature of dissolution in *C. leptoporus* is the separation of the shields resulting in coccosphere collapse (Langer et al 2007). By contrast, in *C. braarudii* and *H. carteri* the earliest dissolution feature is etching leaving the coccospheres intact. Only when coccoliths break due to more pronounced etching do coccospheres collapse in these species (Fig 7). This means that living *C. leptoporus* cells are more vulnerable to dissolution than *C. braarudii / H. carteri* because all three species need a coccosphere to live (Walker et al 2018a, Bianco et al., 2025). While a coccosphere comprised of coccoliths produced by the very cell itself is essential for survival in monospecific cultures of these species, mixed-species coccospheres in natural assemblages indicate that coccosphere integrity can be re-established or modified through incorporation of foreign coccoliths (Johns et al 2023). This might mean that a coccosphere compromised through dissolution or malformation might be repaired by incorporating foreign coccoliths. The protective efficacy of such hybrid coccospheres remains to be tested experimentally. However, the vulnerability sequence described above differs from what would be expected based on species specific coccolith solubility as inferred from sediment samples, which do not suggest that *C. leptoporus* is more vulnerable than *H. carteri* (Berger 1973). Note that we cannot be entirely sure that *C. leptoporus* coccoliths would break faster than *H. carteri* coccoliths when subjected to the same omega calcite because the *C. leptoporus* experiment was conducted at an omega calcite of 0.5 (Langer et al 2007) as opposed to the ca 0.033 used here. Nevertheless, considering the very early appearance of separated

shields in *C. leptoporus* (Langer et al 2007) and the comparatively late appearance of broken coccoliths in *H. carteri*, it is highly likely that coccosphere collapse in *C. leptoporus* would occur earlier than in *H. carteri* (at a given omega calcite). Although bulk surface waters in most parts of the global ocean are currently supersaturated with respect to calcite, ongoing ocean acidification drives the calcite saturation state towards undersaturation which will be reached in some areas, e.g. the Southern Ocean, around the year 2100, posing a threat to calcifying organisms including coccolithophores (Langer and Ziveri 2025). Regardless of the actual threat posed by corrosive waters to living coccolithophores, the argument we are making here centres on relative vulnerability of different species in case of calcite undersaturation.

3.4) *A nanostructure in C. braarudii biomineral*

A nanostructure on the proximal side of the distal shield in *C. braarudii* became visible 3 hours into the experiment (Fig. 6). The individual "units" of this nanostructure are ca. 50-100 nm in diameter. The distal side of the distal shield does not show this nanostructure. Differences between the proximal and distal sides of the distal shield have previously been reported (Henriksen et al 2004, Young et al 2004). Whereas the distal side of the distal shield consists of crystallographic a-faces, the proximal side seems to be more profoundly regulated by the cell and does not show crystallographic faces (Young et al 2004). The nanostructure shown here is what was described as "tuberculate surface" by Henriksen et al. (2004). The latter authors conclude that the tubercles are part of the calcite structure. We confirm this conclusion which is illustrated particularly well by a side view of these tubercles (Fig. 3D). We can only speculate what effect this nanostructure might have on the dissolution resistance / susceptibility of the distal shield elements. Considering that the distal shield elements of C. braarudii are the only coccolith parts of all three species that are still present at the end of the experiment (Fig. 6), it seems clear that they are comparatively dissolution resistant. Whether this resistance stems from the nanostructure or some other feature remains an open question but it is fair to say that the nanostructure does not make coccolith crystals highly susceptible to dissolution. The importance of micro- and nanostructures in differential dissolution behaviour of various biominerals has been recently highlighted in the context of vulnerability to ocean acidification (Langer and Ziveri 2025). It is conceivable that the nanostructure in C. braarudii slows down etching and / or provides structural reinforcement. This scenario would be plausible if the nanostructure was an

418 organo-mineral composite structure as opposed to being composed of calcite only
419 (Walker and Langer 2021). A nanostructure of similar size in $CaCO_3$ biominerals is
420 widespread in extracellular calcifiers, where it is a central indicator of a layered growth
421 mechanism featuring particle accretion which is believed to be non-operative in
422 coccolithophores (Kadan et al 2021, Walker and Langer 2021). It remains, however, an
423 open question whether the nanostructure in *C. braarudii* is similar to that in
424 extracellular calcifiers i.e. whether it is also an organo-mineral composite structure
425 (Walker and Langer 2021). This question is pertinent to coccolithophore
426 biomineralization because an extracellular-like nanostructure in coccoliths would call
427 into question widely held views about crystallization of coccolith crystals (Walker and
428 Langer 2021). However, even if the tuberculate nanostructure in *C. braarudii* should
429 turn out to be extracellular-like, it would still be unclear how it is possible that the distal
430 side of the distal shield is different, i.e. shows crystallographic a-faces and no
431 nanostructure. The standard biomineralization model explaining the nanostructure in
432 extracellular calcifiers cannot account for the difference between the two sides of the
433 distal shield in *C. braarudii*, and neither can the standard model of coccolith
434 biomineralization (Young et al 2004, Walker and Langer 2021). This difference between
435 the proximal and the distal side of the distal shield shows how finely tuned
436 morphogenesis in *C. braarudii* is. We can only speculate how this fine tuning is
437 achieved, but the composition of the organic coating might play a role. The composition
438 of coccolith associated polysaccharides is known to be species specific, but we
439 speculate that it might also be site specific within the coccolith vesicle (Walker et al
440 2018b).

441 **4) Conclusions**

442 In summary, our results show that dissolution experiments complement field studies and
443 contribute to a deeper understanding of both coccolith structure and the ecological
444 impact of seawater undersaturation with respect to calcite. We conclude that

445 1) the most dissolution-resistant species is *C. braarudii*, followed by *H. carteri* and *S.*
446 *apsteinii*;

447 2) structural integrity of the coccosphere under dissolution is highest in *C. braarudii*,
448 followed by *H. carteri* and *S. apsteinii*, with *C. leptoporus* probably showing the
449 weakest coccosphere;

3) we identify dissolution in published field data where it was not recognised;

4) lopadolith R-units dissolve faster than V-units, illustrating that different microstructures in the same coccolith have different dissolution kinetics despite containing the same mineral;

5) the nanostructure in the distal shield of *C. braarudii* points to a fine-tuning in coccolith morphogenesis that is not accounted for by our current model of coccolith biomineralization.

Acknowledgements

No acknowledgements at this stage.

Funding:

Generalitat de Catalunya (MERS, 2021 SGR00640), Spanish Ministry of Science and Innovation (CEX2019-000940-M), and BIOCAL project (PID2020-113526RB-I00, Spanish Ministry of Science and Innovation).

Competing interests

The authors declare no conflict of interests.

Author contributions

GL: conception, experiments, analysis, writing, IP: experiments, writing, JRY: analysis, field samples, writing, PZ: writing.

Data availability

Data will be made available at Pangaea database.

References

Baumann, K.-H., Böckel, B., and Frenz, M.: Coccolith contribution to South Atlantic carbonate sedimentation, in: Coccolithophores, edited by: Thierstein, H. R. and Young, J. R., Springer Berlin Heidelberg, Berlin, Heidelberg, 367–402, https://doi.org/10.1007/978-3-662-06278-4_14, 2004.

Berger WH (1973) Deep-sea carbonates: evidence for a coccolith lysocline. Deep-Sea Res 20:917–921

Bianco, S., Bordiga, M., Langer, G., Ziveri, P., Cerino, F., Di Giulio, A., and Lupi, C. (2025) Low sensitivity of a heavily calcified coccolithophore under increasing CO2: the case study of Helicosphaera carteri, Biogeosciences, 22, 1821–1837, https://doi.org/10.5194/bg-22-1821-2025.

Broecker, W. & Clark, E. Ratio of coccolith CaCO3 to foraminifera CaCO3 in late Holocene deep sea sediments. Paleoceanogr. 24, PA3205 (2009).

Broecker, W. S. & Peng, T.-H. Tracers in the Sea. 690 (Lamont-Doherty Geological Observatory, Columbia University, 1982)

Broerse, A.T.C., Ziveri, P., Honjo, S., (2000) Coccolithophore (CaCO3) flux in the Sea of Okhotsk: seasonality, settling and alteration processes Marine Micropaleontology, 39 (1-4): 179-200.

Burns, D. A. (1977). Phenotypes and dissolution morphotypes of the genus Gephyrocapsa Kamptner and Emiliania huxleyi (Lohmann). New Zealand Journal of Geology and Geophysics, 20(1), 143-155.

Cubillos, J.C., Henderiks, J., Beaufort, L., Howard, W.R., & Hallegraeff, G.M. (2012). Reconstructing calcification in ancient coccolithophores: Individual coccolith weight and morphology of Coccolithus pelagicus (sensu lato). Marine Micropaleontology, 92, 29-39.

Daniels, C., Poulton, A., Young, J., Esposito, M., Humphreys, M., Ribas-Ribas, M., Tynan, E., and Tyrrell, T.: Species-specific calcite production reveals Coccolithus pelagicus as the key calcifier in the Arctic Ocean, Mar. Ecol. Prog. Ser., 555, 29–47, https://doi.org/10.3354/meps11820, 2016.

Daniels, C. J., Sheward, R. M., and Poulton, A. J.: Biogeochemical implications of comparative growth rates of Emiliania huxleyi and Coccolithus species, Biogeosciences, 11, 6915–6925, https://doi.org/10.5194/bg-11-6915-2014, 2014.

Drescher B, Dillaman RM, Taylor AR. (2012) Coccolithogenesis In Scyphosphaera apsteinii (Prymnesiophyceae). J Phycol. 2012 Dec;48(6):1343-61. doi: 10.1111/j.1529-8817.2012.01227.x. Epub 2012 Sep 17. PMID: 27009987.

507 Gafar, N. A., Eyre, B. D., and Schulz, K. G.: Particulate inorganic to organic carbon
508 production as a predictor for coccolithophorid sensitivity to ongoing ocean acidification,
509 Limnol. Oceanogr. Letters, 4, 62–70, https://doi.org/10.1002/lol2.10105, 2019

510 Gerecht AC, Supraha L, Edvardsen B, Langer G, Henderiks J. 2015. Phosphorus
511 availability modifies carbon production in Coccolithus pelagicus (Haptophyta). Journal
512 of Experimental Marine Biology and Ecology 472: 24–31.

513 Guptha, .M., Banerjee, R. & Mergulhao, L. On the nature of the calcareous substrate of
514 a ferromanganese crust from the Vityaz Fracture Zone, Central Indian Ridge: (2002).
515 inferences on paleoceanography. Geo-Mar Lett 22, 12–18 (2002).
516 https://doi.org/10.1007/s00367-002-0091-0

517 Hassenkam, T., Johnsson, A. M. S., Bechgaard, K., & Stipp, S. L. S. (2011). Tracking
518 single coccolith dissolution with picogram resolution and implications for CO2
519 sequestration and ocean acidification. Proceedings of the National Academy of Sciences
520 of the United States of America, 108, 8571-8576.

521 Henderiks, J., Sturm, D., Šupraha, L., & Langer, G. (2022). Evolutionary Rates in the
522 Haptophyta: Exploring Molecular and Phenotypic Diversity. Journal of Marine Science
523 and Engineering, 10(6), 798. https://doi.org/10.3390/jmse10060798

524 Henriksen, K., Young, J. R., Bown, P. R., & Stipp, S. L. S. (2004). Coccolith
525 biomineralisation studied with atomic force microscopy. Palaeontology, 47(3), 725-743.

526 Hoffmann, R., Kirchlechner, C., Langer, G., Wochnik, A. S., Griesshaber, E., Schmahl,
527 W. W., and Scheu, C. (2015) Insight into Emiliania huxleyi coccospheres by focused ion
528 beam sectioning, Biogeosciences, 12, 825–834, https://doi.org/10.5194/bg-12-825-2015,
529 2015.

530 Holcová K, Scheiner F. (2023). An experimental study on post-mortem dissolution and
531 overgrowth processes affecting coccolith assemblages: A rapid and complex process.
532 Geobiology. 2023 Mar;21(2):193-209. doi: 10.1111/gbi.12528. Epub 2022 Oct 11.
533 PMID: 36218003.

534 Honjo,S. 1975. "DISSOLUTION OF SUSPENDED COCCOLITHS IN THE DEEP-
535 SEA WATER COLUMN AND SEDIMENTATION OF COCCOLITH OOZE",
536 Dissolution of Deep-sea Carbonates, William V. Sliter, Allan W. H. Bé, Wolfgang H.
537 Berger

538 Johns, CT et al. Adsorptive exchange of coccolith biominerals facilitates viral infection.
539 Sci. Adv.9, eadc8728(2023). DOI:10.1126/sciadv.adc8728

540 Johnson, R., Langer, G., Rossi, S., Probert, I., Mammone, M., & Ziveri, P. (2022).
541 Nutritional response of a coccolithophore to changing pH and temperature. Limnology
542 and Oceanography, 67(10), 2309-2324.

543 Kadan Y, Tollervey F, Varsano N, Mahamid J, Gal A. (2021) Intracellular nanoscale
544 architecture as a master regulator of calcium carbonate crystallization in marine
545 microalgae. Proc Natl Acad Sci U S A. 2021 Nov 16;118(46):e2025670118. doi:
546 10.1073/pnas.2025670118. PMID: 34772804; PMCID: PMC8694050.

547 Kleijne, A. (1990). Distribution and malformation of extant calcareous nannoplankton
548 in the Indonesian Seas. Marine Micropaleontology, 16(3-4), 293-316.

549 Langer, G. & Benner, I. (2009) Effect of elevated nitrate concentration on calcification
550 in Emiliania huxleyi. J. Nannoplankton Res. 30: 77–80.

551 Langer, G., & Bode, M. (2011). CO2 mediation of adverse effects of seawater
552 acidification in Calcidiscus leptoporus. Geochemistry, Geophysics, Geosystems, 12(5).
553 https://doi.org/10.1029/2010GC003393

554 Langer, G., Geisen, M., Baumann, K. H., Kläs, J., Riebesell, U., Thoms, S., & Young, J.
555 R. (2006). Species-specific responses of calcifying algae to changing seawater
556 carbonate chemistry. Geochemistry, geophysics, geosystems, 7(9).

557 Langer, G., Gussone, N., Nehrke, G., Riebesell, U., Eisenhauer, A., Kuhnert, H., Rost,
558 B., Trimborn, S., & Thoms, S. (2006b). Coccolith strontium to calcium ratios in
559 Emiliania huxleyi: The dependence on seawater strontium and calcium concentrations.
560 Limnology and Oceanography, 51(1 I), 310-320.
561 https://doi.org/10.4319/lo.2006.51.1.0310

562 Langer, G., Nehrke, G., & Jansen, S. (2007). Dissolution of Calcidiscus leptoporus
563 coccoliths in copepod guts? A morphological study. Marine Ecology Progress Series,
564 331, 139-146.

565 Langer, G., Oetjen, K., Brenneis, T. (2013). On culture artefacts in coccolith
566 morphology. Helgoland Marine Research, 67(2), 359-369.
567 https://doi.org/10.1007/s10152-012-0328-x

Langer G, Taylor AR, Walker CE, Meyer EM, Ben Joseph O, Gal A, Harper GM, Probert I, Brownlee C, Wheeler GL. Role of silicon in the development of complex crystal shapes in coccolithophores. New Phytol. 2021 Sep;231(5):1845-1857. doi: 10.1111/nph.17230. Epub 2021 Mar 9. PMID: 33483994.

Langer G, Probert I, Cox MB, Taylor A, Harper GM, Brownlee C, Wheeler G. (2023) The Effect of cytoskeleton inhibitors on coccolith morphology in Coccolithus braarudii and Scyphosphaera apsteinii. J Phycol. 2023 Feb;59(1):87-96. doi: 10.1111/jpy.13303. Epub 2022 Dec 24. PMID: 36380706.

Matsuoka, H. (1990) A new method to evaluate dissolution of CaCO3 in the deep-sea sediments. Trans. Proc. Paleont. Soc. Jpn., 157, 430-434

McIntyre A, McIntyre R (1971) Coccolith concentration and differential solution in oceanic sediments. In: Funnel BM, Riedel WR (eds) The micropaleontology of oceans. Cambridge University Press, Cambridge, p 253–261O

Meyer, Erin M., Langer, Gerald, Brownlee, Colin, Wheeler, Glen L. and Taylor, Alison R. 2020 Sr in coccoliths of Scyphosphaera apsteinii: Partitioning behavior and role in coccolith morphogenesis. Geochimica et Cosmochimica Acta, 285. 41-54. 10.1016/j.gca.2020.06.023

Milliman, J. D. Production and accumulation of calcium carbonate in the ocean: budget of a nonsteady state. Glob. Biogeochemical Cycles 7, 927–957 (1993).

Morse, J. W. & Mackenzie, F. T. Geochemistry of sedimentary carbonates. (Elsevier, 1990).

Pierrot, D., D. Wallace, E. Lewis, R. Wallace, and W. Wallace. (2011) MS Excel Program Developed for CO2 System Calculations. ORNL Environmental Sciences Division. doi:10.3334/CDIAC/otg

Roth PH, Berger WH (1975) Distribution and dissolution of coccoliths in the south and central Pacific. In: Sliter WV, Be AWH, Berger WH (eds) CaCO3 dissolution in the deep sea. Cushman Foundation for Foraminiferal Research, Santa Barbara, CA, p 87–113

596 Roth, P. H., & Coulbourn, W. T. (1982). Floral and solution patterns of coccoliths in
597 surface sediments of the North Pacific. Marine Micropaleontology, 7(1), 1–52.
598 doi:10.1016/0377-8398(82)90014-7

599 Sand, K., Pedersen, C., Sjoberg, S., Nielsen, J., Makovicky, E., and Stipp, S. (2014).
600 Biomineralization: long-term effectiveness of polysaccharides on the growth and
601 dissolution of calcite. Cryst. Growth Des. 14, 5486–5494. doi: 10.1021/cg5006743

602 Subhas, A. V., Rollins, N. E., Berelson, W. M., Erez, J., Ziveri, P., Langer, G., & Adkins,
603 J. F. (2018). The dissolution behavior of biogenic calcites in seawater and a possible
604 role for magnesium and organic carbon. Marine Chemistry, 205, 100-112.
605 https://doi.org/10.1016/j.marchem.2018.08.001

606 Subhas, A. V., Dong, S., Naviaux, J. D., Rollins, N. E., Ziveri, P., Gray, W., Rae, J. W.
607 B., Liu, X., Byrne, R. H., Chen, S., Moore, C., Martell-Bonet, L., Steiner, Z., Antler, G.,
608 Hu, H., Lunstrum, A., Hou, Y., Kemnitz, N., Stutsman, J., … Adkins, J. F. (2022).
609 Shallow Calcium Carbonate Cycling in the North Pacific Ocean. Global
610 Biogeochemical Cycles, 36(5). https://doi.org/10.1029/2022GB007388

611 Sulpis, O., Jeansson, E., Dinauer, A., Lauvset, S. K., & Middelburg, J. J. (2021).
612 Calcium carbonate dissolution patterns in the ocean. Nature Geoscience, 14(6), 423–
613 428. https://doi.org/10.1038/s41561-021-00743-y

614 Walker JM, Langer G. (2021) Coccolith crystals: Pure calcite or organic-mineral
615 composite structures? Acta Biomater. 2021 Apr 15;125:83-89. doi:
616 10.1016/j.actbio.2021.02.025. Epub 2021 Feb 22. PMID: 33631395.

617 Walker JM, Greene HJM, Moazzam Y, Quinn PD, Parker JE, Langer G. (2024) An
618 uneven distribution of strontium in the coccolithophore Scyphosphaera apsteinii
619 revealed by nanoscale X-ray fluorescence tomography. Environ Sci Process Impacts.
620 2024 Jun 19;26(6):966-974. doi: 10.1039/d3em00509g. PMID: 38354057.

621 Walker CE, Taylor AR, Langer G, Durak GM, Heath S, Probert I, Tyrrell T, Brownlee
622 C, Wheeler GL. (2018a) The requirement for calcification differs between ecologically
623 important coccolithophore species. New Phytol. 2018 Oct;220(1):147-162. doi:
624 10.1111/nph.15272. Epub 2018 Jun 19. PMID: 29916209; PMCID: PMC6175242.

625 Walker, Charlotte E., Heath, Sarah, Salmon, Deborah L., Smirnoff, Nicholas, Langer,
626 Gerald, Taylor, Alison R., Brownlee, Colin and Wheeler, Glen L. (2018b) An

627 extracellular polysaccharide-rich organic layer contributes to organization of the
628 coccosphere in coccolithophores. Frontiers in Marine Science, 5 (AUG), [306].
629 (doi:10.3389/fmars.2018.00306).

630 Wheeler GL, Sturm D, Langer G. (2023) Gephyrocapsa huxleyi (Emiliania huxleyi) as a
631 model system for coccolithophore biology. J Phycol. 2023 Dec;59(6):1123-1129. doi:
632 10.1111/jpy.13404. Epub 2023 Nov 20. PMID: 37983837.

633 Yang M, Batchelor-McAuley C, Barton S, Rickaby REM, Bouman HA, Compton RG.
634 (2021) Opto-Electrochemical Dissolution Reveals Coccolith Calcium Carbonate
635 Content. Angew Chem Int Ed Engl. 2021 Sep 13;60(38):20999-21006. doi:
636 10.1002/anie.202108435. Epub 2021 Aug 15. PMID: 34288323; PMCID:
637 PMC8518593.

638 Young, J. R. (1994). Variation in *Emiliania huxleyi* coccolith morphology in samples
639 from the Norwegian EHUX experiment, 1992. Sarsia. 79(4): 417-425.

640 Young, J. R. (2008). Scyphosphaera porosa Kamptner 1967 rediscovered in the
641 plankton. Journal of Nannoplankton Research. 30(1): 35-38

642 Young, J. R., Henriksen, K., & Probert, I. (2004). Structure and morphogenesis of the
643 coccoliths of the CODENET species. In Coccolithophores: From molecular processes to
644 global impact, Thierstein, H. R., & Young, J. R. (Eds.), Springer, 191-216.

645 Ziveri, P., Baumann, K.H., Böckel, B. Bollmann, J. and Young, J. (2004) Present day
646 coccolithophore-biogeography in the Atlantic Ocean in Thierstein, H. and Young, J.
647 Eds. Coccolithophores: From Molecular Processes to Global Impact. Springer Verlag:
648 403-428.

649 Ziveri, P., De Bernardi, B., Baumann, K.-H., Stoll, H. M., and Mortyn, P. G.: Sinking of
650 coccolith carbonate and potential contribution to organic carbon ballasting in the deep
651 ocean, Deep-Sea Res. Pt. II, 54, 659–675, https://doi.org/10.1016/j.dsr2.2007.01.006,
652 2007.

653 Ziveri, P., Gray, W. R., Anglada-Ortiz, G., Manno, C., Grelaud, M., Incarbona, A., Rae,
654 J. W. B., Subhas, A. V., Pallacks, S., White, A., Adkins, J. F., & Berelson, W. (2023).
655 Pelagic calcium carbonate production and shallow dissolution in the North Pacific
656 Ocean. Nature Communications, 14(1), 805. https://doi.org/10.1038/s41467-023-36177-
657 w

Ziveri, P., Passaro, M., Incarbona, A., Milazzo, M., Rodolfo-Metalpa, R., & Hall-Spencer, J. M. (2014). Decline in Coccolithophore Diversity and Impact on Coccolith Morphogenesis Along a Natural CO 2 Gradient. The Biological Bulletin, 226(3), 282–290. https://doi.org/10.1086/BBLv226n3p282

Fig 1

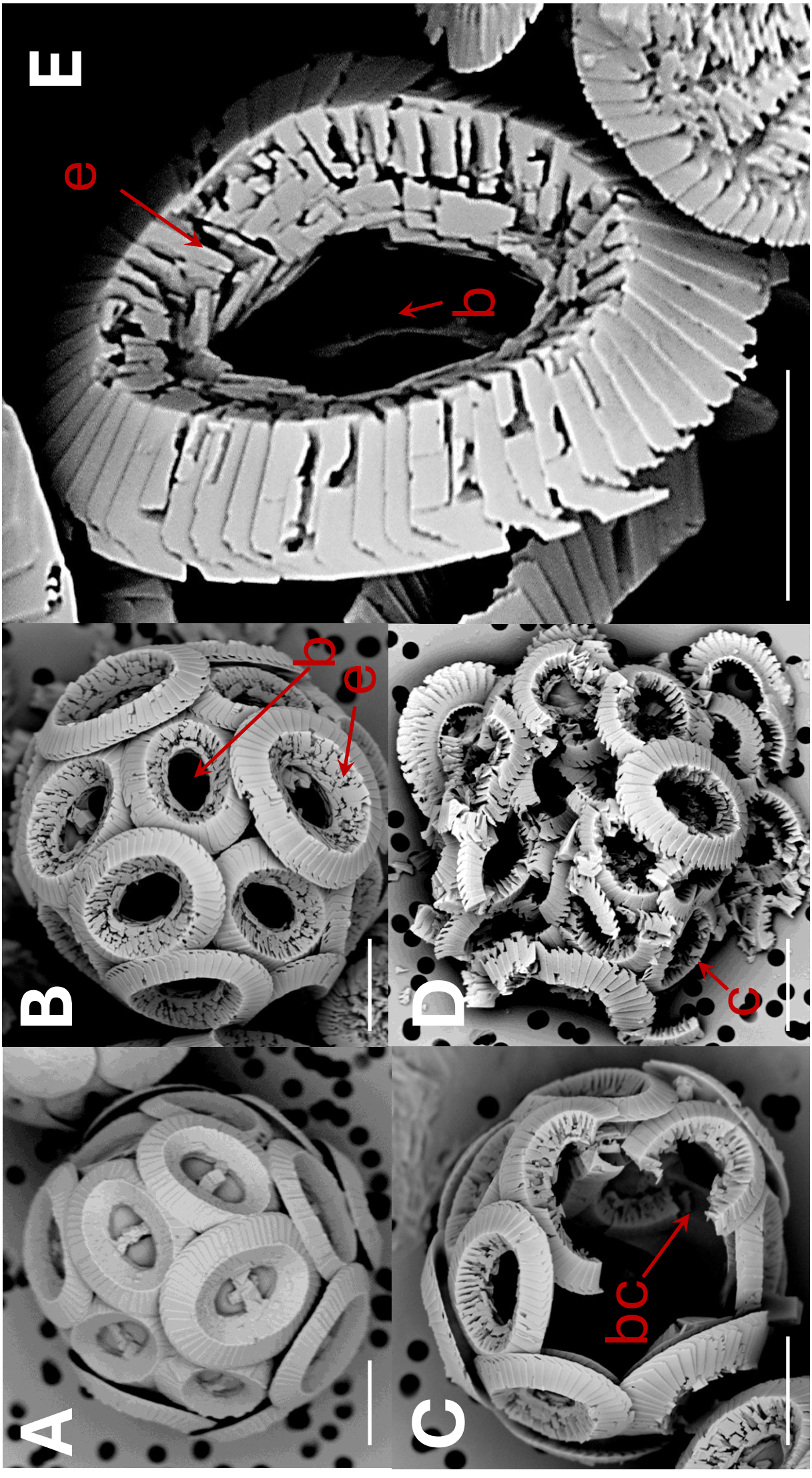

Fig 1 *Coccolithus braarudii*

A) coccosphere at t0, no dissolution. Scale bar 5µm. B) coccosphere; etching (e) of tube and distal shield and central area bar missing (b). Scale bar 5µm. C) broken coccoliths (bc), etching of tube, central bar missing and gaps in coccosphere. Scale bar 5µm. D) collapsed coccosphere (c), also showing etching (e) of tube and distal shield and central area bar missing (b). Scale bar 5µm. E) coccolith, etching (e) of tube and distal shield, and central area bar missing (b). Note that the etching consistently occurs by opening of sutures between elements rather than by dissolution of element surfaces. Scale bar 3µm.

Fig 2

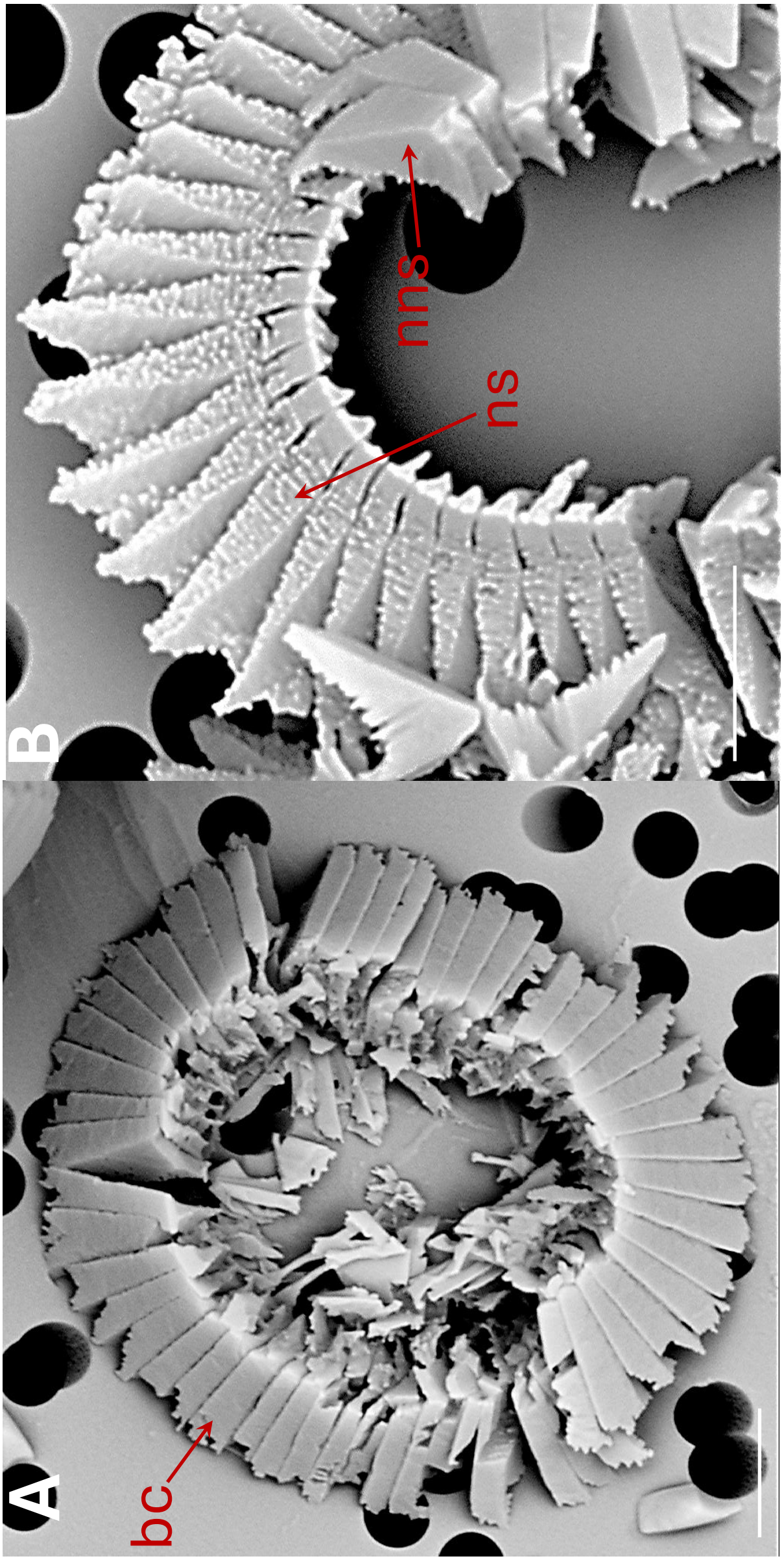

Fig 2 *Coccolithus braarudii*

A) broken coccolith (bc) distal shield in distal view. B) broken coccolith proximal view of distal shield showing nanostructure (ns); the arrow indicates isolated distal shield elements in distal view, from another coccolith, not displaying nanostructure (nns) on distal and vertical surfaces. All scale bars 2µm.

Fig 3

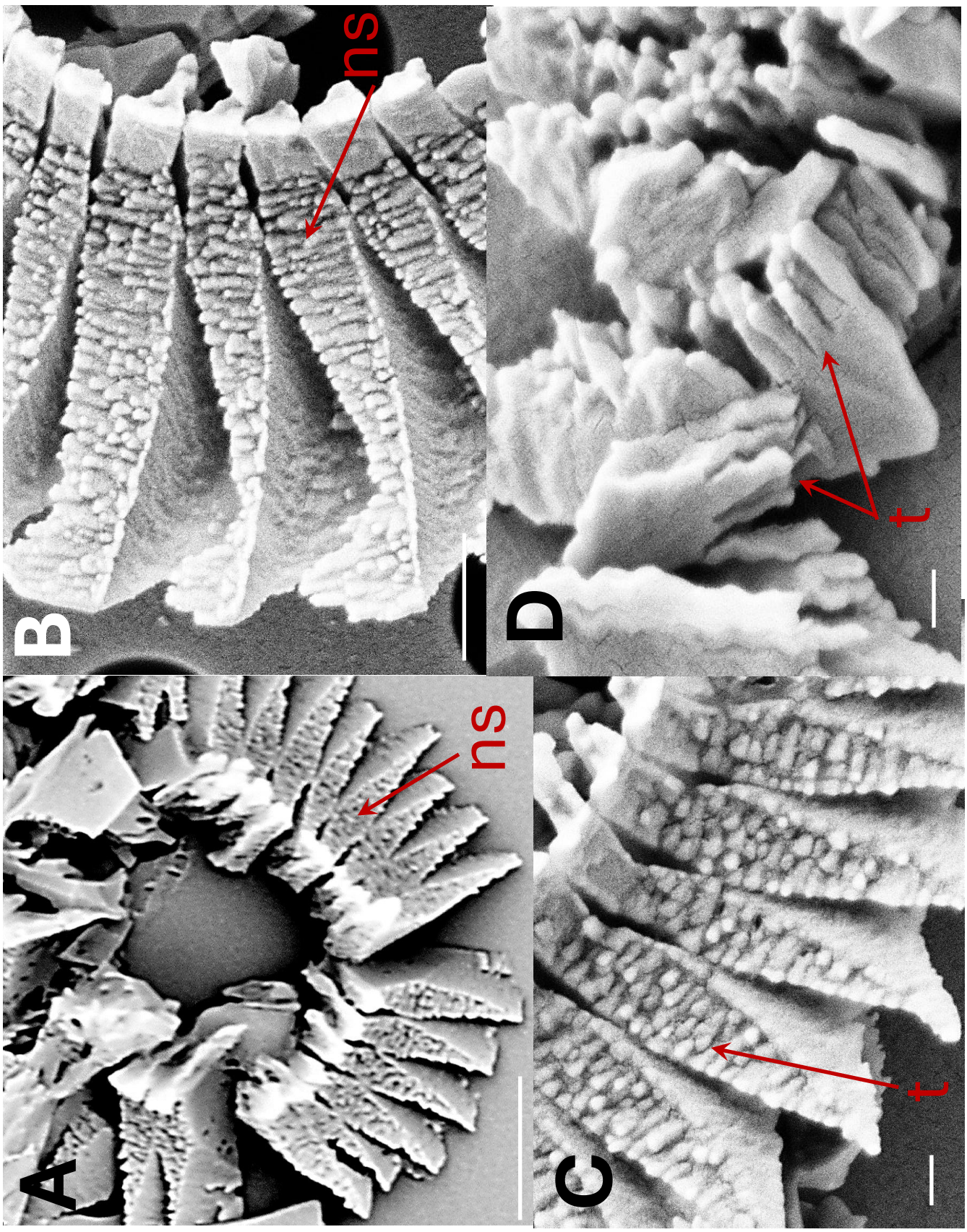

Fig 3 *Coccolithus braarudii*

A) broken coccolith distal shield in proximal view showing nanostructure (ns). Scale bar 2µm B) proximal view of distal shield elements showing nanostructure (ns). Scale bar 500nm. C) proximal view of distal shield elements showing nanostructure (ns); individual "tubercles“ (t) of the nanostructure are ca 50-100nm, Scale bar 200nm. D) isolated distal shield elements showing nanostructure "tubercles“ (t) in vertical side view (arrow). Scale bar 200nm.

Fig 4

Fig 4 *Helicosphaera carteri*

A) coccosphere at t0, no dissolution. Scale bar 5µm. B) coccosphere displaying coccoliths with severe etching (e) and a broken coccolith (bc). Scale bar 5µm. C) collapsed coccosphere including broken coccoliths (bc). Scale bar 5µm. D) coccoliths in distal view with etching (e) in flange and blanket. Scale bar 3µm. E) coccolith in distal view with etching in flange and blanket. Scale bar 2µm. F) coccolith in proximal view with etching (e) in flange. Scale bar 5µm.

Fig 5

Fig 5 *Scyphosphaera apsteinii*

A) coccosphere at t0, no dissolution B) lopadolith base etching (be); murolith centre missing (cm) C) lopadolith barrel etching (re) and serrated rim (sr) D and E) broken lopadoliths F) isolated V-units G) murolith at t0, no dissolution H) murolith with etching (me) I) lopadolith in distal view showing R- and V-units (R- and V arrows, Young 2008); and broken murolith (bm). All scale bars 5µm.

Fig 6

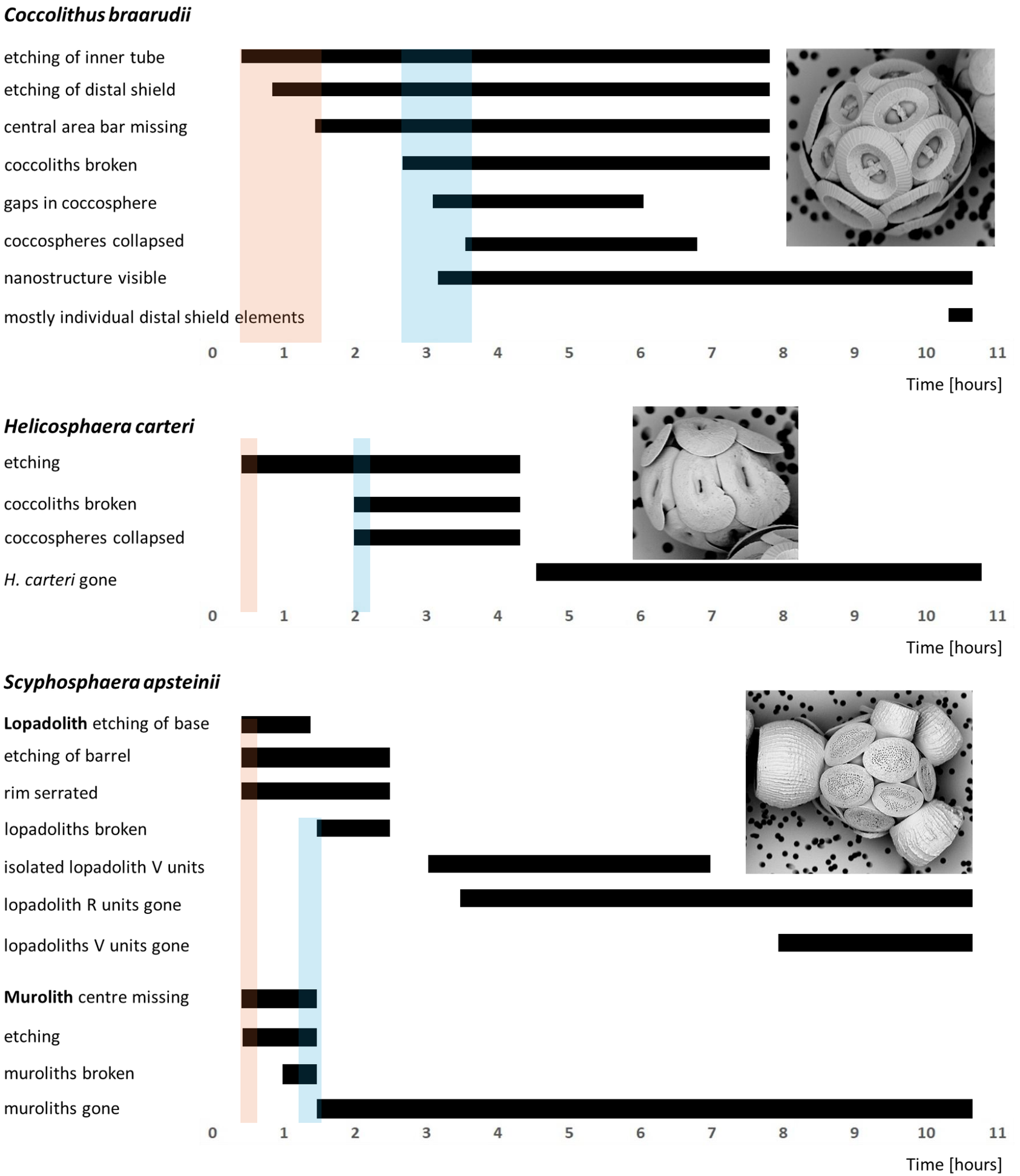
Coccolithus braarudii
etching of inner tube
etching of distal shield
central area bar missing
coccoliths broken
gaps in coccosphere
coccospheres collapsed
nanostructure visible
mostly individual distal shield elements
0 1 2 3 4 5 6 7 8 9 10 11
Time [hours]
Helicosphaera carteri
etching
coccoliths broken
coccospheres collapsed
H. carteri gone
0 1 2 3 4 5 6 7 8 9 10 11
Time [hours]
Scyphosphaera apsteinii
Lopadolith etching of base
etching of barrel
rim serrated
lopadoliths broken
isolated lopadolith V units
lopadolith R units gone
lopadoliths V units gone
Murolith centre missing
etching
muroliths broken
muroliths gone
0 1 2 3 4 5 6 7 8 9 10 11
Time [hours]

Fig 6 Timelines of dissolution. Bars indicate the period during which the respective feature can be observed. Shaded backgrounds indicate the onset points of major features. Pink backgrounds indicate the onset of etching, blue backgrounds indicate the onset of breakage/collapse. For example-images of each feature see Figs 1-5.

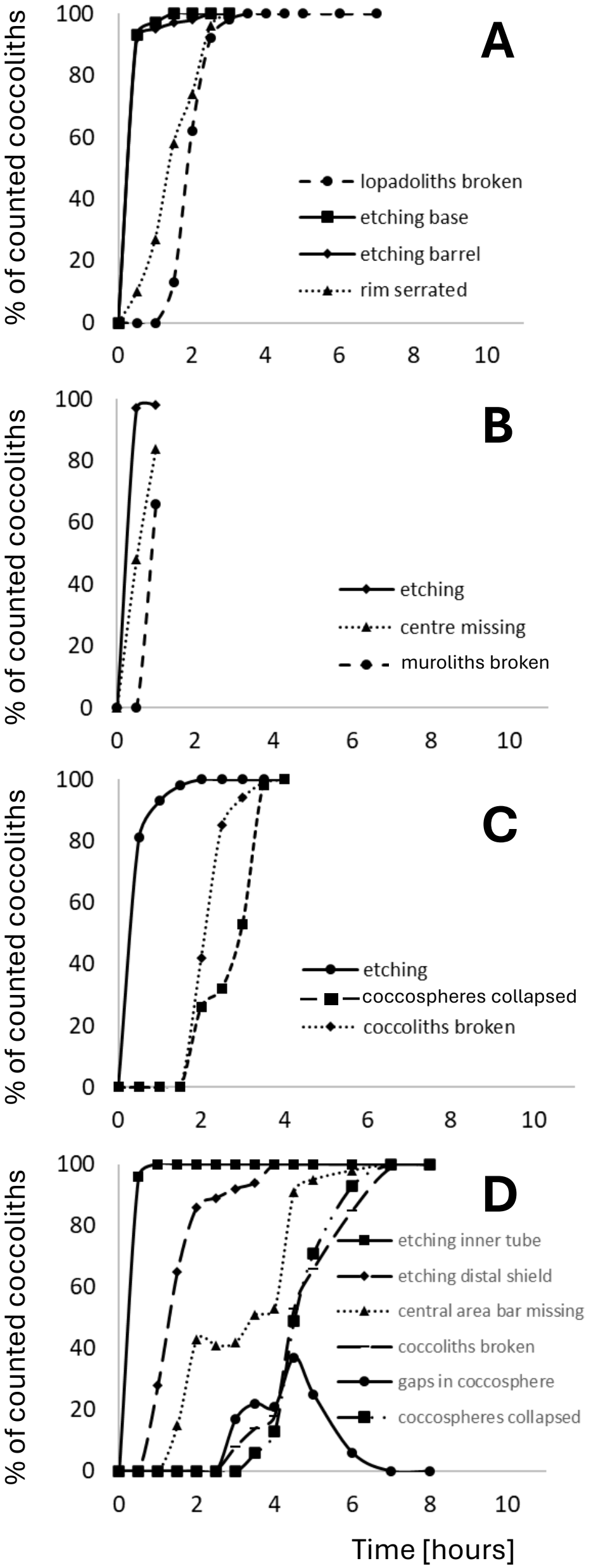
A
% of counted coccoliths
100
80
60
40
20
0
0
2
4
6
8
10
lopadoliths broken
etching base
etching barrel
rim serrated
B
% of counted coccoliths
100
80
60
40
20
0
0
2
4
6
8
10
etching
centre missing
muroliths broken
C
% of counted coccoliths
100
80
60
40
20
0
0
2
4
6
8
10
etching
coccospheres collapsed
coccoliths broken
D
% of counted coccoliths
100
80
60
40
20
0
0
2
4
6
8
10
etching inner tube
etching distal shield
central area bar missing
coccoliths broken
gaps in coccosphere
coccospheres collapsed
Time [hours]

Fig 7 Quantification of the observations illustrated in Fig 6. Plotted is the percentage of each analysed feature versus time in hours from start of experiment. A) *Scyphosphaera apsteinii* lopadoliths B) *Scyphosphaera apsteinii* muroliths C) *Helicosphaera carteri* D) *Coccolithus braarudii*

Fig 8

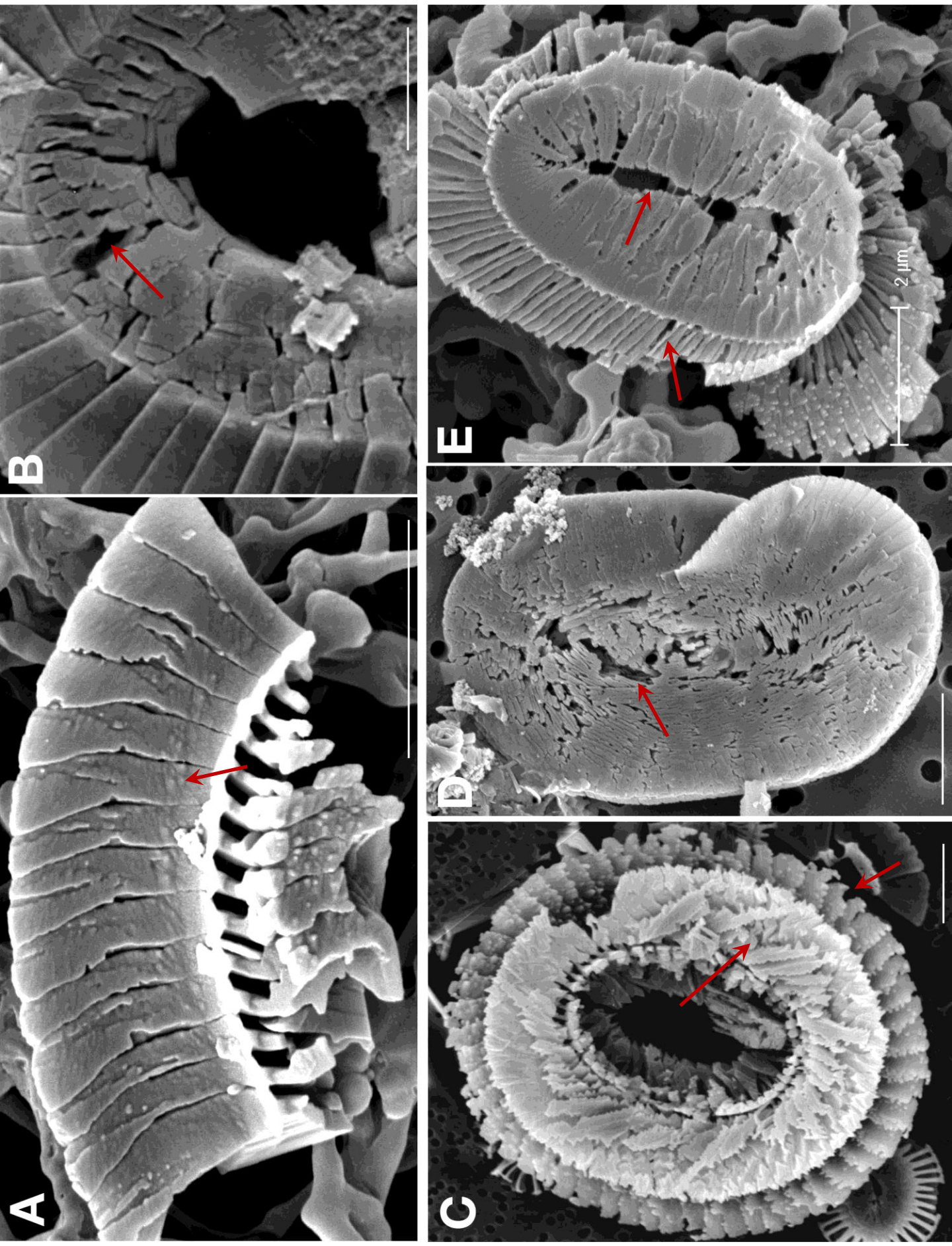

Fig 8 Field samples showing etching patterns comparable to those seen in the experimental samples (arrows). All scale bars 2 µm.

Coccolithus braarudii: A) Lower surface of a broken piece of distal shield showing nanostructure. B) Central area of distal shield showing early stage dissolution. C) Proximal surface showing advanced dissolution.

Helicosphaera carteri: D) Distal Surface showing early stage dissolution. E) Proximal surface showing advanced dissolution.

A, B - sediment trap samples from 3200m, N. Atlantic; C - surface water sample, NW Atlantic; D- sediment trap sample, Canaries, 200m; E plankton sample from 120m, Gulf of Mexico.